Article

Optical fibre gripper for high-performance 3D micromanipulation

https://doi.org/10.1038/s41586-026-10673-7

Received: 24 July 2025

Accepted: 18 May 2026

Published online: 17 June 2026

Check for updates

Deng Pan[1,2], Kaiwen Liang[2], Chen Xin[2], Lei Zhong[2], Shaojun Jiang[2], Chenchu Zhang[3]✉, Liang Yang[2], Zhiqiang Wang[1], Zhaoxin Lao[3], Jincheng Ni[2], Chaowei Wang[2]✉, Jiawen Li[2], Shenglai Zhen[1], Benli Yu[1], Zhixiang Huang[1], Fang-Wen Sun[2], Jiaru Chu[2], Yanlei Hu[2]✉, Li Zhang[4] & Dong Wu[1,2]✉

Optical tweezers offer precise, non-contact control, but operate in a limited force regime and impose strict requirements on the characteristics of the targets as well as the environmental conditions[1–4]. Millimetre-scale mechanical tweezers can offer higher gripping force but are not suitable for precise manipulations[5–11]. Integrating microgrippers directly at the optical fibres provides a new approach for precise micromanipulation. However, existing fibre-integrated tweezers still face challenges in achieving high-performance manipulation of micro-objects (for example, single cells) within narrow spaces, mainly due to simplified architectures, constrained designs and millimetre-scale footprints[12–14]. Here we report a three-dimensional (3D) optical fibre gripper (OFG), which is fabricated by two-step, two-photon polymerization. The OFG consists of rigid photoresist microclaws and soft thermoresponsive hydrogel muscle doped with silver nanoparticles, and its size is only 38 × 38 × 61 μm^3. The OFG exhibits a force-to-mass ratio of about 340 μN mg^{-1}, outperforming previously reported fibre-integrated tweezers by one to two orders of magnitude. The OFG can manipulate opaque particles, irregular micromechanical components and diverse single-cell types. We further demonstrated its potential in 3D microassembly of complex microdevices (bearings, shafts and gearboxes) and biomimetic sampling in the narrow environment (<300 μm). These results position the OFG as a compact fibre-tip manipulator for 3D micromanipulation, offering reversible and tunable gripping in an intermediate force regime between optical field trapping and millimetre-scale mechanical tweezers.

Microscale object manipulation, including single-cell manipulation[15–17], microstructure assembly[18,19] and microdevice transfer[20,21], is of great significance in the fields of biomedical engineering, micro-electro-mechanical systems and micro- and nanophotonics. Among existing micromanipulation strategies, microgrippers (microtweezers) have attracted considerable interest owing to their compact structure, versatile actuation mechanisms and ease of system integration. However, most mechanically, magnetically or pneumatically and hydraulically driven microtweezers exhibit relatively large structural footprints[5–11], which hampers their ability to achieve high-precision manipulation at the single-cell scale and precludes operation in confined spaces smaller than about 300 μm. By contrast, optical tweezers enable non-contact, high-precision manipulation and are widely used for microscale and sub-microscale objects, particularly those below approximately 1 μm (refs. 4,22). However, because they rely on light trapping[1], their usable forces are typically in the piconewton range, which limits stable manipulation of heavy or opaque structures.

Optical fibres offer excellent light transmission, mechanical flexibility and a compact form factor[23–27], making them an attractive platform for integrating microtweezers aimed at high-performance micro- and nanomanipulation. Recent studies have demonstrated fibre-integrated micromanipulation by incorporating light-responsive materials (such as hydrogels and liquid crystal elastomers) at the fibre tip using approaches, including self-rolling[12], mechanical embedding[13,14] and ultraviolet (UV) curing techniques[28]. However, most existing fibre-based microtweezers rely on a single constituent material. Rigid material provides mechanical robustness but lacks deformability, whereas soft materials enable large deformation yet typically suffer from slow response and low force-to-mass ratios, thereby limiting their gripping performance. Moreover, optical-fibre-based microtweezers at present are generally large-sized (ranging from about 270 μm to

[1]State Key Laboratory of Opto-Electronic Information Acquisition and Protection Technology, Key Laboratory of Opto-Electronic Information Acquisition and Manipulation of Ministry of Education, Information Materials and Intelligent Sensing Laboratory of Anhui Province, School of Optoelectronic Science and Engineering, Anhui University, Hefei, China. [2]CAS Key Laboratory of Mechanical Behaviour and Design of Materials, Key Laboratory of Precision Scientific Instrumentation of Anhui Higher Education Institutes, Department of Precision Machinery and Precision Instrumentation, University of Science and Technology of China, Hefei, China. [3]School of Mechanical Engineering, School of Instrument Science and Opto-Electronics Engineering, Anhui Province Key Lab of Aerospace Structural Parts Forming Technology and Equipment, Hefei University of Technology, Hefei, China. [4]Department of Mechanical and Automation Engineering, Chinese University of Hong Kong, Hong Kong, People's Republic of China. ✉e-mail: hfutzcc@hfut.edu.cn; chaoweiw@ustc.edu.cn; huyl@ustc.edu.cn; dongwu@ustc.edu.cn

several millimetres) and predominantly two-dimensional (2D) planar structures, which makes it challenging to achieve high-precision manipulation of complex or irregular microtargets at the single-cell scale.

To address these challenges, we report an integrated three-dimensional (3D) optical fibre gripper (OFG), which consists of a rigid photoresist 'skeleton' and a soft thermoresponsive hydrogel 'muscle' doped with silver nanoparticles. On near-infrared laser illumination delivered through the optical fibre, the doped silver nanoparticles convert light energy into heat, triggering constraint-induced anisotropic deformation of the hydrogel and thereby actuating the grippers. The OFG is directly fabricated on the end face of commercial optical fibre by two-step femtosecond laser two-photon polymerization (2PP). Despite its compact footprint ($38 \times 38 \times 61\ \mu m^3$), the device exhibits a fast actuation response (76.7 ms) and a high force-to-mass ratio of about 340 $\mu N\ mg^{-1}$, representing a one or two orders of magnitude improvement over previously reported fibre-integrated actuators. We further demonstrate reliable manipulation of single cells, sub-10-μm irregular objects, as well as 3D assembly of complex microstructures. Moreover, owing to its compact structure, the OFG enables high-precision minimally invasive sampling in confined bile duct, highlighting its potential as a versatile micromanipulation platform for biomedicine applications and micro- and nanomanufacturing.

Structural design of OFG

In the biological musculoskeletal system, precise motion control arises from the coordinated operation of two core modules[29]: (1) contraction force generation by muscle tissues and (2) mechanical force transfer by skeletal structures. Inspired by this model, we designed a bioinspired OFG, in which optical fibre acts as an energy-delivery channel, transmitting external energy to the OFG, soft thermoresponsive hydrogel doped with silver nanoparticles mimics the 'muscle' for the driving force generation, and rigid photoresist microclaws act as a 'bone' for mechanical output (Fig. 1a). The OFG is directly manufactured on the cleaved facet of a multimode optical fibre (50 μm core diameter and 125 μm cladding diameter) using 2PP. The resulting OFG features a compact 3D architecture with overall dimensions of $38 \times 38 \times 61\ \mu m^3$ (Fig. 1b,c), well matched to microscale manipulation tasks, such as effective grasping and release of single cells or sub-10-μm targets.

The opening and closing of the OFG are regulated by near-infrared laser illumination delivered through the optical fibre. In the absence of laser, the hydrogel remains hydrated and swollen, maintaining the mirotweezers in a closed state (Fig. 1d and Supplementary Video 1). On illumination with the 808 nm laser, the doped silver nanoparticles convert the laser energy into heat, inducing rapid hydrogel contraction and consequently opening the microtweezers. In this design, the optical fibre serves as a guided energy-delivery pathway, and the hydrogel-photoresist composite structure converts the absorbed light into mechanical work, forming an integrated fibre-tip microsystem with a bioinspired skeleton–muscle architecture.

Photothermal actuation of OFG

OFG was constructed in situ on the cleaved facet of a multimode optical fibre by a two-step 2PP process that sequentially fabricates the rigid photoresist microclaws and the soft thermoresponsive hydrogel doped with silver nanoparticles (Methods, section '2PP-based 3D fabrication of OFG'; Supplementary Figs. 1, 2, 7–10; and Supplementary Video 2). The working mechanism of OFG relies on the synergistic response of thermosensitive hydrogel and photothermal nanomaterials (Fig. 2a). The hydrogel network is doped with silver nanoparticles with excellent photothermal conversion ability. In the swollen state, the 3D polymer network of the hydrogel is stabilized by extensive hydrogen bonding with water molecules, resulting in volumetric expansion that maintains the gripper in a closed configuration. On irradiation with a near-infrared laser, the embedded silver nanoparticles rapidly convert light energy into heat, leading to a localized temperature increase. This photothermal heating disrupts the hydrogen-bonding interactions between the polymer chains and water molecules, triggering water expulsion from the polymer network and pronounced gel contraction, which mechanically drives the opening of the OFG.

For the hydrogel muscle structure, we selected 20 mW and 400 nm voxel spacing as representative fabrication parameters to obtain well-formed structures with notable swelling response in water (Supplementary Fig. 3a). The thermoresponsive properties of the hydrogel are measured using a temperature-controlled platform, with a swelling rate ranging from −0.23 to 0.1 (Supplementary Fig. 3b). Notably, the low critical response temperature of the hydrogel lies within the physiological temperature range compatible with cell viability, providing a thermal operating window suitable for safe single-cell manipulation. The mechanical properties of the rigid microclaws can be controllably tuned by adjusting the processing energy of SZ2080 (Supplementary Fig. 3c).

The deformation behaviour of the composite microstructure was governed by the mechanical properties of the soft thermally responsive hydrogel and the rigid photoresist (Supplementary Figs. 4 and 5). The microclaw consists of three arms (Supplementary Fig. 6) anchored to the fibre end through a column of 6 μm diameter. Compared with two- or four-arm configurations (Supplementary Fig. 11), the three-claw configuration achieves a better balance between gripping performance and fabricating complexity, with higher practicality and stability.

The optical actuation performance was characterized by coupling an 808 nm near-infrared laser into the distal end of the optical fibre and recording the microclaws motion at 4,352 frames per second (Fig. 2b). After laser irradiation for 1.15 ms, the hydrogel began to respond. The OFG reached 75% of its maximum opening stroke (14.9 μm) within 76.7 ms, and subsequently stabilized within 1 s, with an opening distance of 19.9 μm. On laser off, the microclaws retract from the maximum opening to 14.9 μm within about 105 ms, followed by a further recovery to near-zero displacement within around 429 ms. Periodic actuation was further evaluated under varying drive frequencies with a fixed laser pulse width of 80 ms. As the driving frequency increased, the opening–closing stroke gradually decreased (Supplementary Video 3). When the frequency was less than 5 Hz, the OFG maintained 75% of the maximum opening and closing stroke (Fig. 2c). Higher frequencies caused incomplete recovery and smaller stroke. Moreover, no obvious degradation was observed over 910 consecutive cycles (Fig. 2d and Supplementary Video 4). Extended 48 h endurance tests show stable actuation for $>8.7 \times 10^4$ cycles under typical driving powers (Supplementary Information section 2 and Supplementary Figs. 12–14).

Owing to the composite material structure design, our OFG outperforms previously reported optical fibre-based microtweezers in terms of response speed (76.7 ms) and operating frequency (5 Hz). By contrast, traditional fibre-integrated microtweezers based on single-material systems typically operate at about 1 Hz (refs. 12,14,28), and exhibit slower response, which limits their applicability in rapid micromanipulation.

Coupled optical–thermal–mechanical multiphysics simulation further verified the response characteristics of the OFG under different laser powers (Fig. 2e,f, Supplementary Information section 3 and Supplementary Video 5). At a laser power of 29 mW, the hydrogel shrank to its designed state, resulting in zero net displacement. Beyond this threshold, the opening–closing stroke increased with the input power. At 205 mW, the experimentally measured displacement was 22 μm, compared with a simulated value of 23 μm, showing good agreement. Notably, the required power depends on nanoparticle loading: high-density silver nanoparticles reduce the actuation power to 6–8 mW, markedly suppressing laser leakage. The hydrogel can also be doped with other photothermal nanoparticles (for example, Fe_3O_4, excitation wavelength 1,060 nm) to shift actuation wavelength,

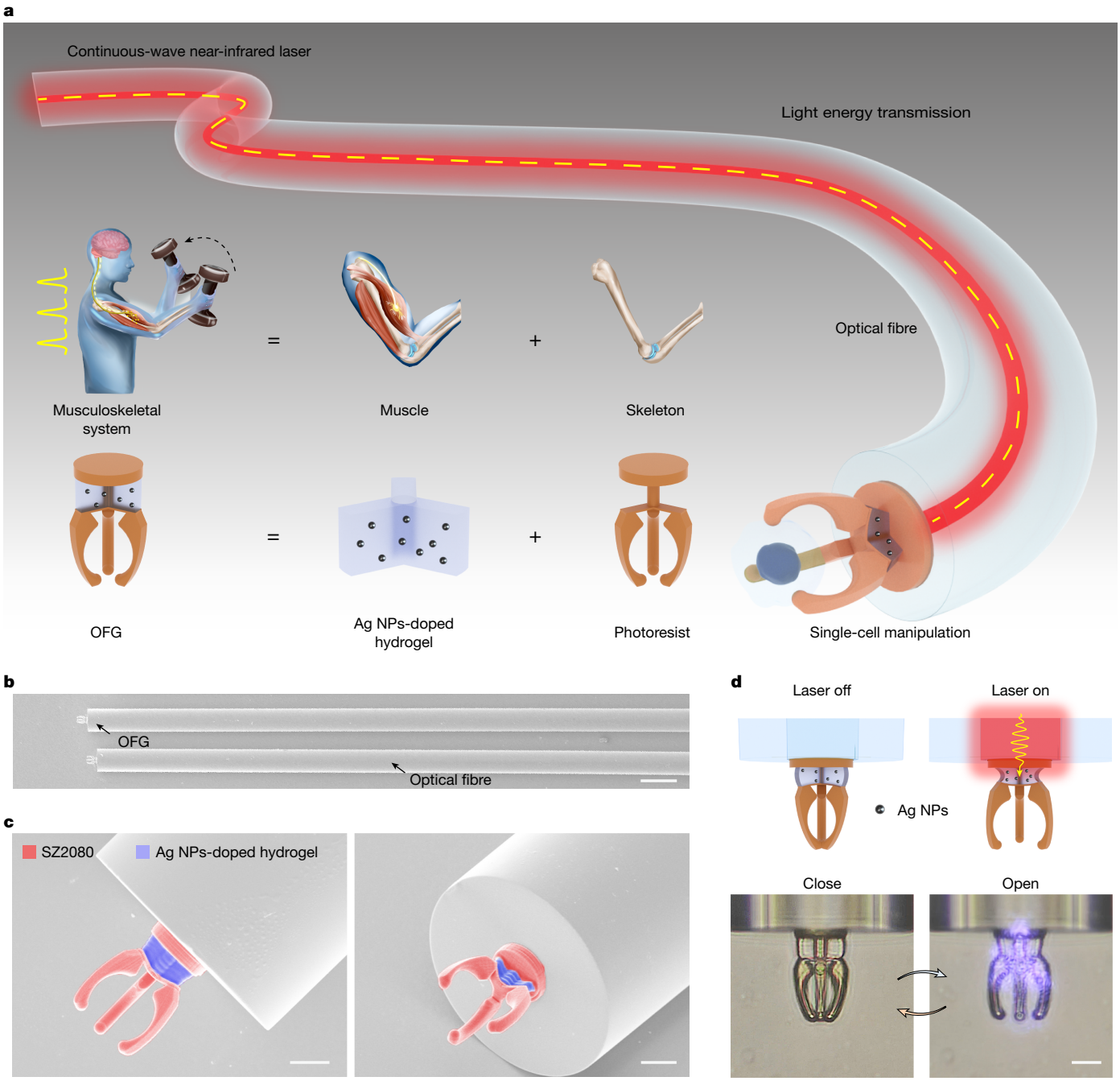

Fig. 1 | Bioinspired muscle–bone structural design of 3D OFG. a, Bioinspired design: a thermoresponsive hydrogel acts as an artificial muscle, a rigid SZ2080 scaffold provides the skeleton. **b**, SEM image of an OFG fabricated on the cleaved facet of an optical fibre. **c**, Top-view and 45°-tilted view SEM images highlight the 3D claw geometry. **d**, Actuation of OFG. Embedded Ag nanoparticles (NPs) photothermally heat the hydrogel. Laser off: the swollen hydrogel keeps the claws closed; laser on: hydrogel contraction opens the claws. Scale bars, 200 µm (**b**); 20 µm (**c**,**d**).

providing additional pathways to improve laser safety (Supplementary Figs. 15 and 16).

High-performance manipulation by OFG

Leveraging its rapid actuation and precise control, the OFG enables a series of microscale manipulation tasks (Fig. 3a). Here, an *XYZ* stage was used to position target objects (positioning module), whereas an *XZθ* stage was used for the position control of OFG (end-effector module). An 808 nm semiconductor laser delivered optical excitation from the opposite end of the optical fibre, while the entire operation processes were recorded by two cameras (Supplementary Fig. 17). The manipulation sequence consisted of four steps: (1) target approach (laser off, OFG closed); (2) target capture (laser on, OFG opened and aligned with the silica ball, then turned off the laser to achieve gripping); (3) transport (laser off) and (4) target release (laser on). The 3D translation stages were mainly used for spatial control to provide stable and repeatable positioning, whereas the OFG enabled gripping and releasing. If necessary, vibration can be applied to assist in detaching from the target (Supplementary Figs. 18–20). Notably, OFG operation requires only a compact semiconductor fibre laser, offering a streamlined experimental setup. By contrast, conventional pneumatic and hydraulic drive systems typically rely on bulky and complex external devices (such as pressure controllers, vacuum controllers[30,31]), and

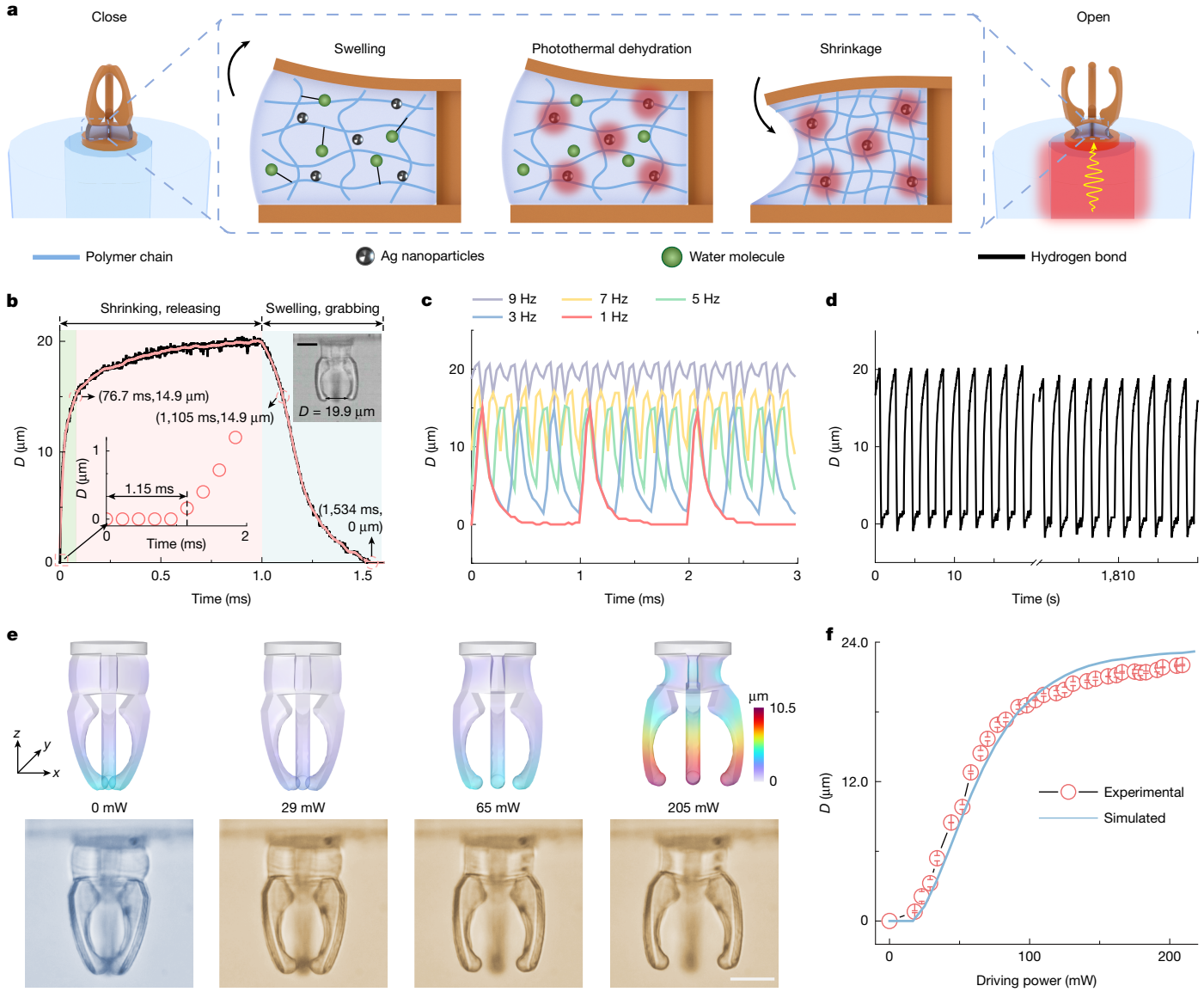

Fig. 2 | Fibre integration and photothermal actuation of 3D composite material OFG. a, Schematic of the working mechanism of the OFG. **b**, Deformation of the OFG as a function of time during one operation cycle. The inset is an optical image of the OFG at 1 s. **c**, Deformation response characteristics in the OFG at different drive frequencies. **d**, Fatigue testing of the OFG, demonstrating more than 900 operation cycles without notable performance attenuation. **e**, Comparison of simulation (top) and experimental (bottom) results for OFG deformation under different driving laser powers. **f**, Simulated and experimental deformation curves of OFG devices at different driving energies. Data are presented as mean ± s.d., $n = 3$ in **f**. Scale bars, 20 μm (**b**,**e**).

these microtweezers are generally limited to manipulating objects larger than 50 μm, which restricts flexible handling of morphologically complex targets at the subcellular scale.

Beyond transparent silica spheres, OFG can also capture opaque and irregular objects (Fig. 3b). We successfully captured and released alumina spheres of various sizes (diameter 9–24 μm; Supplementary Video 6), suggesting that the reflectance of the grasped object does not affect the performance of the device. Moreover, the OFG can also manipulate irregular micro- and nanotargets, including silicon carbide microfragments, polymer microrings and micropentagonal stars. However, owing to geometric and mechanical constraints of the current design, the OFG is not suitable for manipulating submicron objects (≤1 μm) or for operating in fully enclosed spaces.

Leveraging the flexible and precise manipulation abilities of OFG, we achieved programmable microscale assembly operations. We arranged the target particles in a binary format (1 = with microsphere and 0 = without microsphere) within three 1 × 3 grids and successfully spelt out 'AHU' (Fig. 3c, Supplementary Fig. 21 and Supplementary Video 7). Beyond planar manipulation, OFG also enables accurate placement of microspheres at different heights (0 μm, 20 μm and 40 μm above the substrate; Supplementary Video 8), demonstrating 3D manipulation abilities (Fig. 3d).

To quantify the net lifting force delivered to an external load (the axial component of the resultant gripping forces and friction), we fabricated an on-chip microspring force sensor (Fig. 3e). Using a bead attached to the microspring (Supplementary Video 9), we found that the spring elongation decreases with increasing driving power (Fig. 3g), corresponding to a net axial lifting force of 0–3.4 μN (0–70 μm elongation; Supplementary Information section 6 and Supplementary Fig. 22). In this test, the OFG operates in a partially closed state because the bead–microspring geometry prevents microbead from being fully seated between the claws.

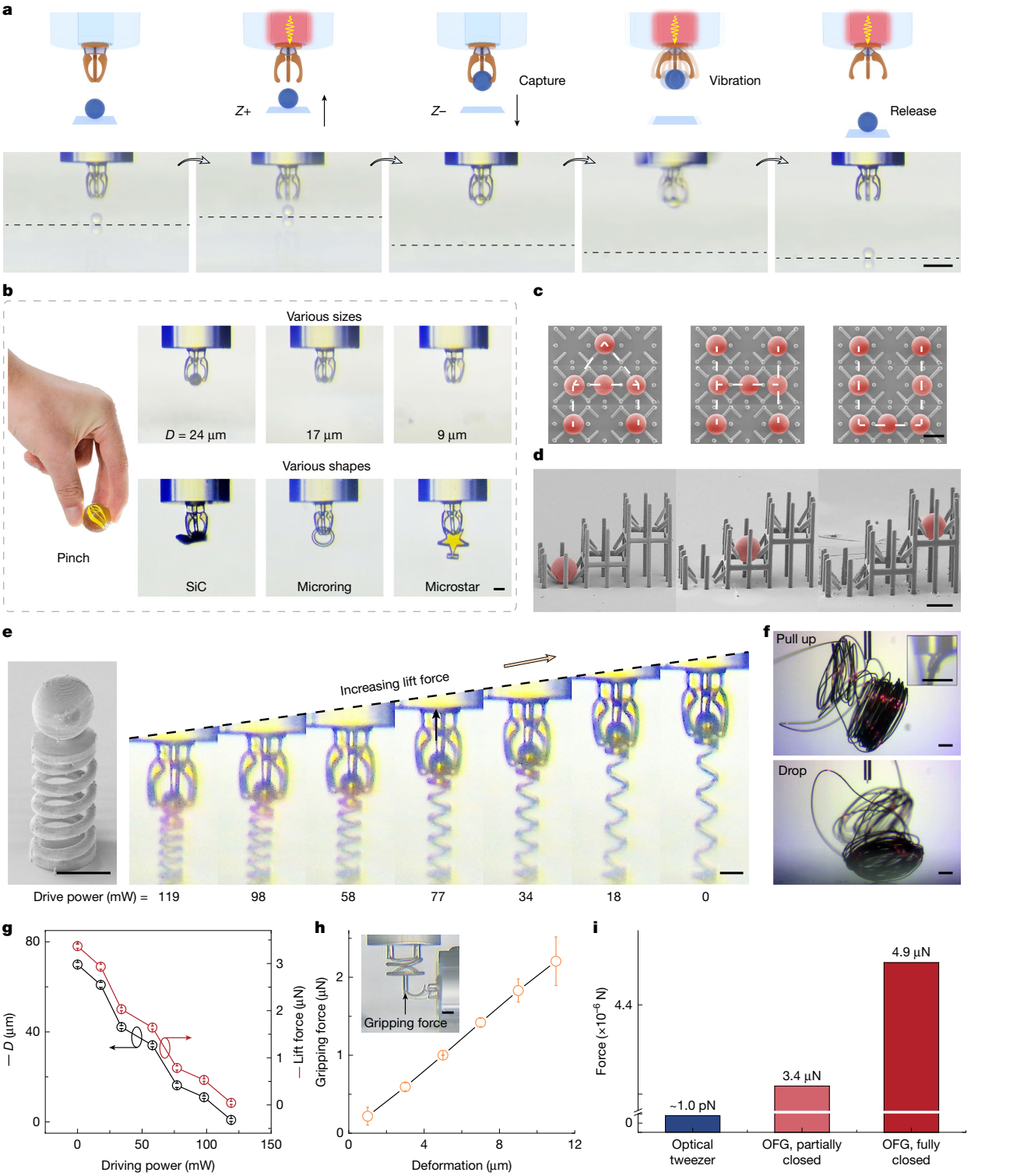

Fig. 3 | High-performance 3D manipulation of opaque, irregular and centimetre-length objects using the OFG. a, Schematics of a typical process of the micro-object manipulation process using the OFG (top) and the corresponding optical images (bottom). **b**, Manipulation of microscopic objects using the OFG mimics the pinching function of human hands. OFGs can handle various micro-objects, including Al_2O_3, microspheres of different sizes, SiC microparticles, microrings and microstars. **c**, Pattern manipulation of SiO_2 microspheres using the OFG. **d**, Manipulation of SiO_2 microspheres in three dimensions using the OFG. **e**, OFG applies a clamping force to the microspheres to create friction, which is used to stretch and deform the microsprings. **f**, The OFG can pull up copper wires with a length of 20 cm and a diameter of 20 μm. **g**, Relationships among the microspring deformation, lift force and driving laser power. The lift force was not measured independently, but calculated from the displacement *D* according to Hooke's law. **h**, The gripping force of OFG measurement by a custom-made microspring probe. **i**, Comparison of the amount of force that an optical tweezer and OFG can exert on an object. Data are presented as mean ± s.d., $n = 3$ in **g** and **h**. Scale bars, 50 μm (**a**); 20 μm (**b**–**e**,**h**); 250 μm (**f**), 100 μm (**f**, top-right inset).

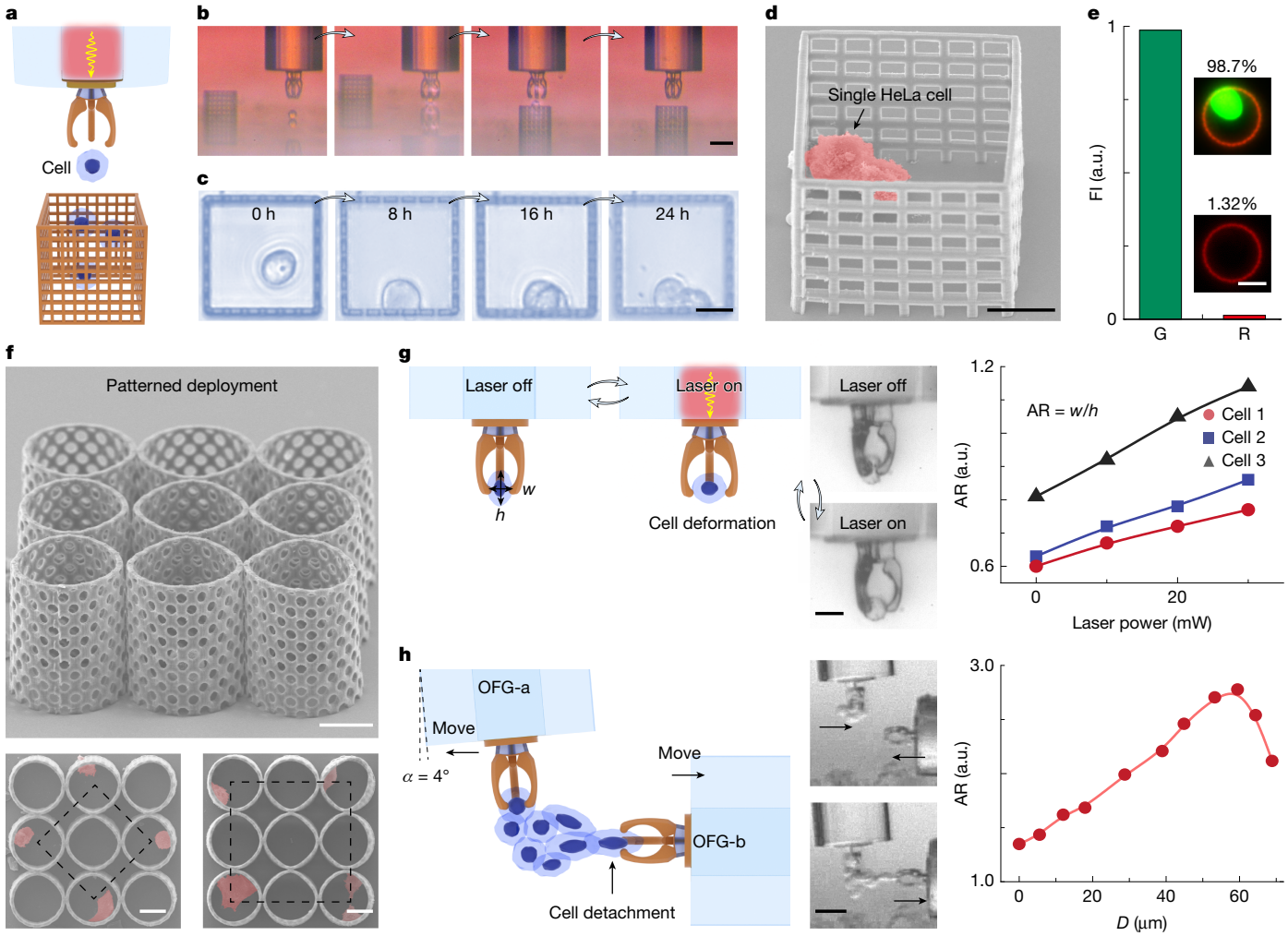

Fig. 4 | Single-cell 3D delicate micromanipulation based on OFG. a, Schematic of single-cell manipulation using the OFG. **b**, Sequential process of manipulating a single HeLa cell, driving laser power of 60–80 mW. **c**, Culture progression of manipulated single HeLa cells over 24 h. **d**, SEM image of manipulated HeLa cell. **e**, Fluorescence intensity (FI) of 120 manipulated HeLa cells. **f**, SEM image of microstructure arrays designed for cell manipulation. The cells were patterned and placed at eight designated sites. **g**, Cell deformation during OFG gripping at different driving laser powers. **h**, Cooperative single-cell detachment using two OFGs; the plot on the right shows the cell aspect ratio (AR) as a function of the pulling displacement of OFG-b. Scale bars, 50 μm (**b**,**h**); 20 μm (**c**–**g**).

In the fully closed state, the OFG can exhibit greater load capacity. In this state, the OFG successfully lifted copper wire of length 20 cm and diameter 20 μm (Fig. 3f and Supplementary Video 10), corresponding to a net pulling force of about 4.9 μN (Fig. 3i). Noting that the device–fibre bonding strength is about 8.92 mN (Supplementary Fig. 23), indicating that the measured net lifting force in the fully closed state is not interface-limited but constrained by the current claw geometry. Structural optimization could therefore further increase the lifting capacity.

Considering that the device mass is only about 14.3 ng, its force-to-mass ratio is as high as about 340 μN mg^{-1}, which is at least an order of magnitude higher than that of existing optical fibre actuators (Supplementary Table 2). The larger force-to-mass ratio means that the small-sized OFG can not only manipulate μm-sized targets with high precision but also has the load capacity for targets of millimetre to centimetre scale, highlighting the unique advantages of the hydrogel-photoresist composite microstructure in load capacity.

The gripping force of OFG can be defined as the normal contact force exerted by the claw tips on the surface of the grasped object. Using calibrated microspring probes, we measured a peak gripping force of about 2.2 μN per claw (Fig. 3h, Supplementary Information section 8 and Supplementary Figs. 24–26). Because claw deformation is continuously tunable using the drive laser power, the effective gripping force can be adjusted in a grey-scale manner, which is particularly relevant for handling delicate objects such as living cells.

The OFG featured a single-cell-scale structure dimensions, millisecond-level response time and micronewton-level output force, supporting programmable 3D manipulation of complex microtargets, and offering a universal platform for various future micromanipulation applications, such as microassembly (Supplementary Information section 9, Supplementary Fig. 27 and Supplementary Videos 11 and 12).

Delicate single-cell manipulation by OFG

The OFG has adjustable driving force, compact structure size and flexible manipulation mode, which makes it very suitable for single-cell processing tasks (Fig. 4a). In the study of cell migration, differentiation and cell-microenvironment interaction, it is crucial to achieve accurate and non-destructive placement of single cells[32–34]. By emulating the pinching action of human fingers, OFG enables targeted capture, transfer and release of single cells.

Here, HeLa cells were used as a representative human cell line with well-characterized and reproducible biophysical properties[35]. After trypsin treatment, the cells were transformed into suspended spherical individuals, which were captured and transferred into cell microcages one by one by OFG under a driving power of 60–80 mW. (Fig. 4b and

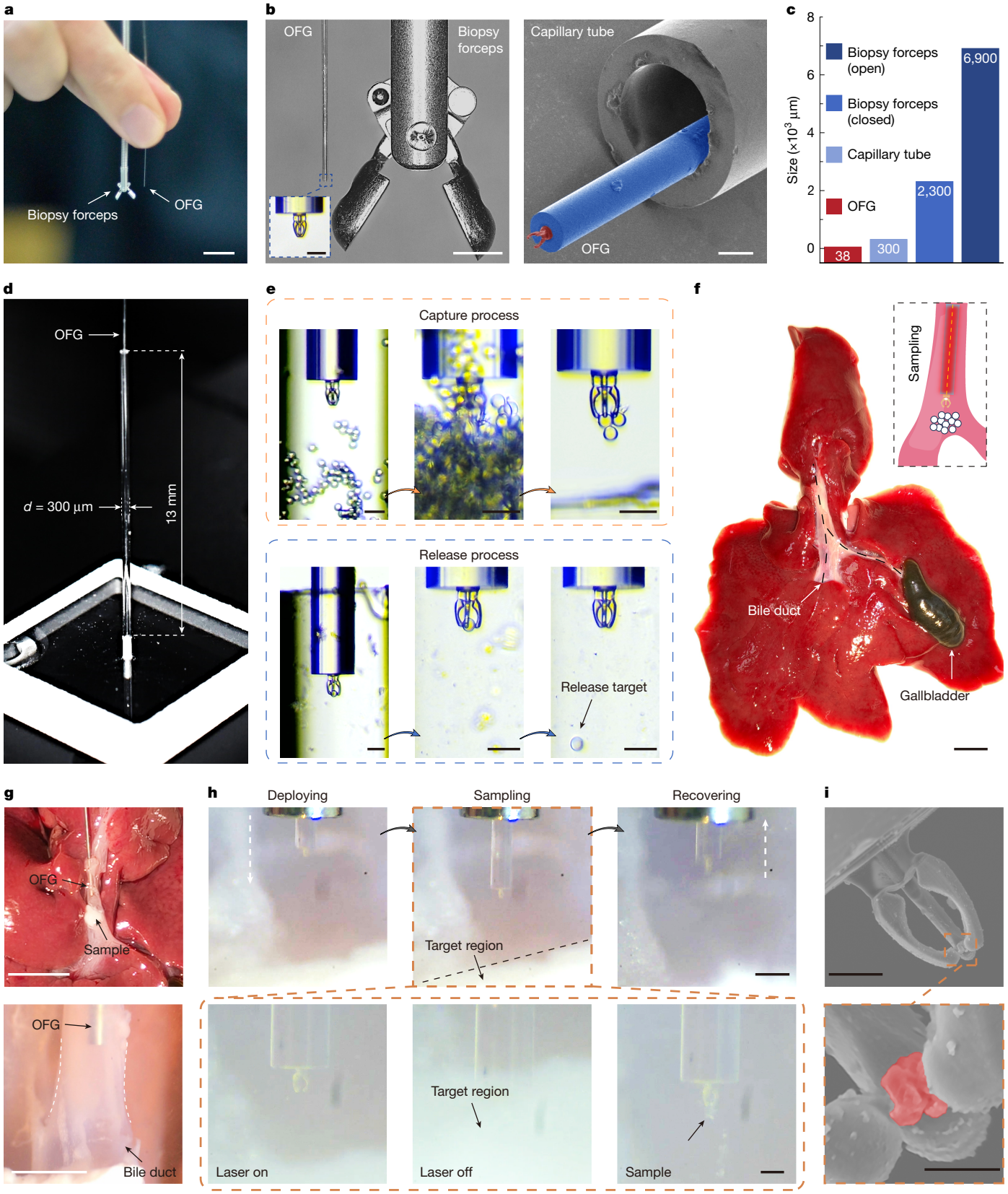

Fig. 5 | Sampling in narrow environment with OFG. a,**b**, Comparison of the OFG with biopsy forceps and capillary tubes. **c**, Comparison of the diameters of the OFG, capillary glass tube and biopsy forceps. **d**, Experimental setup showing the OFG inserted into a capillary tube with a length of 13 mm and width of 0.3 mm for object manipulation. **e**, The release and capture processes of OFG manipulation. **f**, Schematic of the collection of samples from a freshly excised rabbit hepatobiliary specimen using the OFG. **g**, The stainless steel catheter is inserted into the bile duct and advanced towards the target region. **h**, OFG-based sampling process inside the bile duct lumen. **i**, SEM images of the OFG with the sample, which is coloured red in the magnified view. Scale bars, 10 mm (**a**,**f**,**g**, top); 2 mm (**b**, left; **g**, bottom); 50 μm (**b**, inset; **e**; **h**, bottom); 100 μm (**b**, right); 200 μm (**h**, top); 20 μm (**i**, top); 5 μm (**i**, bottom).

Supplementary Video 13). The captured cells subsequently exhibited normal adhesion and spreading and division during culture (Fig. 4c,d and Supplementary Fig. 28). To quantify viability after the full grasp–transfer–release procedure, we increased the sample size to 120 cells. After 4 h incubation (37 °C, 5% CO_2), Calcein-AM/PI staining yielded 98.7% viability by fluorescence statistics and 99.2% by manual counting (Fig. 4e and Supplementary Fig. 29). Apart from HeLa cells, other cell types, including fibroblasts (3T3), thyroid cells (Nthy-ori 3-1) and colorectal cancer cells (Caco-2), were also manipulated with high viability, further demonstrating the broad applicability of the OFG for high-viability, single-cell manipulation across various cell types (Supplementary Fig. 30).

We demonstrated precise patterning manipulation by using 2PP to print 3 × 3 scaffold arrays (Fig. 4f), placing single HeLa cells at predefined positions. The scanning electron microscopy (SEM) images confirmed successful cell adhesion and growth, with some cells completing division, further validating that the OFG manipulation did not compromise cell function (Supplementary Fig. 31).

Apart from binary on–off actuation, the OFG could provide grey-scale control of the grasping interaction, enabling controllable cell deformation. As shown in Fig. 4g, the cell aspect ratio (width to height) increased from 0.81 at 0 mW (maximum closing force) to 1.14 at 30 mW, indicating that maintaining a finite drive power can partially counterbalance the elastic restoring force and thus soften the grasp in a continuous manner. Furthermore, we demonstrated the cooperative operation of two OFGs to isolate individual cells from a cell cluster. One OFG (angled to avoid interference) held the cell cluster, whereas the other OFG gripped a single cell and pulled a single cell free (Fig. 4h and Supplementary Video 14). The cell aspect ratio increases with pulling displacement and peaks at detachment, followed by partial recovery.

Moreover, we demonstrate the versatility of the platform, including stable single-cell capture under fast flow (up to about 7,500 μm s^{-1}) and two distinct puncture modes: (1) a sharpened-tip OFG directly punctures the cell membrane and (2) a standard OFG grips a cell and precisely delivers it onto a pre-positioned sharp microneedle for substrate-assisted puncture (Supplementary Fig. 32).

These results indicate that OFG can realize the non-damaging manipulation of single cells in 3D space, providing a powerful tool and platform support for studying the mechanical behaviour, motility characteristics and differentiation of single cells in artificial microenvironments.

Sampling in narrow environment by OFG

With its compact dimensions (38 × 38 × 61 $μm^3$) and subcellular spatial manipulation ability, the OFG is well suited for operation in confined environments that are inaccessible to conventional biopsy tools. Compared with commercial biopsy forceps (diameter of about 2.3 mm), the OFG is approximately 20-fold smaller in diameter (Fig. 5a), even thinner than the jaws of an ant (Supplementary Fig. 33), and can smoothly pass through a glass capillary with an inner diameter of only 300 μm (Fig. 5b,c). To experimentally evaluate OFG performance in confined spaces, we constructed a glass capillary model with a length of 13 mm and an inner diameter of 300 μm (Fig. 5d). The OFG successfully traversed capillary and reached its distal end, at which it captured and released 15 μm diameter silica microspheres (Fig. 5e). These results demonstrate the ability of OFG to manipulate object in narrow environments, such as gripping cells or thrombus in sub-millimetre capillaries, a task that remains challenging for conventional, larger-scale tweezers.

Moreover, we performed sampling operations using the OFG in freshly excised rabbit bile ducts (Supplementary Video 15). Figure 5f shows the photograph of the liver, gallbladder and bile duct after removal. A stainless steel catheter with an outer diameter of 0.51 mm and an inner diameter of 0.27 mm was used as a protective sheath, and the OFG was deployed through the catheter. After advancing the catheter to the target area (Fig. 5g), the OFG was opened by laser activation, brought into contact with the target by stage translation, and then closed by laser to grasp it (Fig. 5h). The target was then extracted from the bile duct lumen. Subsequent SEM images show that the sample is captured at the tip of the OFG (Fig. 5i, pseudo-coloured red). Moreover, image-guided catheter navigation (for example, X-ray), together with controlled OFG extension and retraction, enables a feasible pathway towards future in vivo studies (Supplementary Fig. 34). These results demonstrate that the OFG enables precise picking, placement and sampling within narrow spaces, highlighting its potential for minimally invasive operation in anatomical structures.

Discussion

Here we report an optical fibre tip gripper that integrates a rigid photoresist skeleton with a soft, thermoresponsive hydrogel muscle doped with silver nanoparticles, forming a compact optically driven micromanipulation platform. The OFG exhibits millisecond-scale actuation (76.7 ms), micronewton-level clamping force (4.9 μN) and an overall footprint of only 38 × 38 × 61 $μm^3$, resulting in an exceptionally high force-to-mass ratio of 340 μN mg^{-1}. This value exceeds that of previously reported fibre-integrated microtweezers[12–14,28] by more than an order of magnitude, and surpasses conventional optical tweezers by three to five orders of magnitude[1,2]. Importantly, the OFG eliminates the need for bulky external actuation apparatus and enables scalable fabrication based on standard commercial optical fibres.

Beyond basic capture and release functions, the biomimetic three-claw architecture enables reliable manipulation of opaque and irregular micro-objects and supports the assembly of complex mocrocomponents. Moreover, the OFG enables delicate single-cell manipulation and can perform high-precision sampling in confined spaces.

This fibre-tip platform supports extensive morphological customization of the microgrippers (Supplementary Fig. 35). Furthermore, the fibre-based OFG is inherently compatible with a broad range of positioning platforms (including robotic arms and endoscopic systems), as well as medical image guidance, enabling operation across complex postures and trajectories and thereby establishing a pathway towards integrated and multifunctional manipulation systems. Collectively, these abilities highlight broad application potential in microassembly, single-cell manipulation, minimally invasive interventions and microsurgery.

Online content

Any methods, additional references, Nature Portfolio reporting summaries, source data, extended data, supplementary information, acknowledgements, peer review information; details of author contributions and competing interests; and statements of data and code availability are available at https://doi.org/10.1038/s41586-026-10673-7.

1. Volpe, G. et al. Roadmap for optical tweezers. *J. Phys. Photon.* **5**, 022501 (2023).
2. Zhang, H. & Liu, K.-K. Optical tweezers for single cells. *J. R. Soc. Interface* **5**, 671–690 (2008).
3. Omine, R., Masui, S., Kadoya, S., Michihata, M. & Takahashi, S. Manipulation of large, irregular-shape particles using contour-tracking optical tweezers. *Opt. Lett.* **49**, 2773–2776 (2024).
4. Bustamante, C. J., Chemla, Y. R., Liu, S. & Wang, M. D. Optical tweezers in single-molecule biophysics. *Nat. Rev. Methods Primers* **1**, 25 (2021).
5. He, C. et al. Magnetically actuated dexterous tools for minimally invasive operation inside the brain. *Sci. Robot.* **10**, eadk4249 (2025).
6. Eom, J. et al. MOGrip: gripper for multiobject grasping in pick-and-place tasks using translational movements of fingers. *Sci. Robot.* **9**, eado3939 (2024).
7. Zhao, Y. et al. Advanced pneumatic microgripper for versatile biomedical micromanipulation. *Precis. Eng.* **88**, 223–234 (2024).
8. Feng, B., Liu, Y., Zhang, J., Qu, S. & Yang, W. Miniature origami robot for various biological micromanipulations. *Nat. Commun.* **16**, 2633 (2025).
9. Nitta, T., Wang, Y., Du, Z., Morishima, K. & Hiratsuka, Y. A printable active network actuator built from an engineered biomolecular motor. *Nat. Mater.* **20**, 1149–1155 (2021).
10. Wu, S. et al. High-load shape memory microgripper with embedded resistive heating and magnetic actuation. *Adv. Funct. Mater.* **35**, 2421798 (2025).

11. Li, X. et al. Porous magnetic soft grippers for fast and gentle grasping of delicate living objects. *Adv. Mater.* **36**, 2409173 (2024).
12. Zong, Y. et al. Waveguide microactuators self-rolled around an optical fiber taper. *Adv. Mater.* **37**, 2418316 (2025).
13. Wani, O. M., Zeng, H. & Priimagi, A. A light-driven artificial flytrap. *Nat. Commun.* **8**, 15546 (2017).
14. Xiao, J. et al. Optical fibre taper-enabled waveguide photoactuators. *Nat. Commun.* **13**, 363 (2022).
15. Tang, F. et al. RNA-Seq analysis to capture the transcriptome landscape of a single cell. *Nat. Protoc.* **5**, 516–535 (2010).
16. Shakoor, A., Gao, W., Zhao, L., Jiang, Z. & Sun, D. Advanced tools and methods for single-cell surgery. *Microsyst. Nanoeng.* **8**, 47 (2022).
17. Zheng, J. et al. 4D printed soft microactuator for particle manipulation via surrounding medium variation. *Small* **20**, e2311951 (2024).
18. Zhang, M., Pal, A., Lyu, X., Wu, Y. & Sitti, M. Artificial-goosebump-driven microactuation. *Nat. Mater.* **23**, 560–569 (2024).
19. Chang, W. et al. Concurrent self-assembly of RGB microLEDs for next-generation displays. *Nature* **617**, 287–291 (2023).
20. Xu, H. et al. 3D nanofabricated soft microrobots with super-compliant picoforce springs as onboard sensors and actuators. *Nat. Nanotechnol.* **19**, 494–503 (2024).
21. Linghu, C. et al. Universal SMP gripper with massive and selective capabilities for multiscaled, arbitrarily shaped objects. *Sci. Adv.* **6**, eaay5120 (2020).
22. Barredo, D., Lienhard, V., de Léséleuc, S., Lahaye, T. & Browaeys, A. Synthetic three-dimensional atomic structures assembled atom by atom. *Nature* **561**, 79–82 (2018).
23. Bian, P. et al. Femtosecond laser 3D nano-printing for functionalization of optical fiber tips. *Laser Photon. Rev.* **18**, 2300957 (2024).
24. Principe, M. et al. Optical fiber meta-tips based on partial-phase control. *Adv. Opt. Mater.* **13**, 2500263 (2025).
25. Yermakov, O. et al. Fiber-based angular demultiplexer using nanoprinted periodic structures on single-mode multicore fibers. *Nat. Commun.* **16**, 2294 (2025).
26. Ren, H. et al. An achromatic metafiber for focusing and imaging across the entire telecommunication range. *Nat. Commun.* **13**, 4183 (2022).
27. Power, M., Thompson, A. J., Anastasova, S. & Yang, G.-Z. A monolithic force-sensitive 3D microgripper fabricated on the tip of an optical fiber using 2-photon polymerization. *Small* **14**, e1703964 (2018).
28. Zmyślony, M. et al. Optical pliers: micrometer-scale, light-driven tools grown on optical fibers. *Adv. Mater.* **32**, 2002779 (2020).
29. Kerkman, J. N., Daffertshofer, A., Gollo, L. L., Breakspear, M. & Boonstra, T. W. Network structure of the human musculoskeletal system shapes neural interactions on multiple time scales. *Sci. Adv.* **4**, eaat0497 (2018).
30. Power, M., Barbot, A., Seichepine, F. & Yang, G.-Z. Bistable, pneumatically actuated microgripper fabricated using two-photon polymerization and oxygen plasma etching. *Adv. Intell. Syst.* **5**, 2200121 (2023).
31. Barbot, A., Power, M., Seichepine, F. & Yang, G.-Z. Liquid seal for compact micropiston actuation at the capillary tip. *Sci. Adv.* **6**, eaba5660 (2020).
32. Wang, C. et al. Microclaw Array Fabricated by single exposure of femtosecond airy beam and self-assembly for regulating cell migratory plasticity. *ACS Nano* **17**, 9025–9038 (2023).
33. Fendler, C. et al. Microscaffolds by direct laser writing for neurite guidance leading to tailor-made neuronal networks. *Adv. Biosyst.* **3**, 1800329 (2019).
34. Fan, S. et al. Accelerating neurite growth and directing neuronal connections constrained by 3D porous microtubes. *Nano Lett.* **22**, 8991–8999 (2022).
35. Masters, J. R. HeLa cells 50 years on: the good, the bad and the ugly. *Nat. Rev. Cancer* **2**, 315–319 (2002).

Methods

Materials

Standard silver nitrate titration solution was purchased from Codow. *N*-isopropylacrylamide, *N*,*N*′-methylenebisacrylamide, diphenyl (2,4,6-trimethylbenzoyl) phosphine oxide, polyvinylpyrrolidone K30 and ethylene glycol were purchased from Aladdin. The SZ2080 photoresist was purchased from IESL-FORTH. Multimode optical fibres (core diameter 50 µm, cladding 125 µm) were purchased from YOFC. All chemicals were used as received without further purification.

Preparation of the hydrogel precursor

The hydrogel precursor was prepared by dissolving 400 mg of *N*-isopropylacrylamide, 30 mg of *N*,*N*′-methylenebisacrylamide, 30 mg of diphenyl(2,4,6-trimethylbenzoyl)phosphine oxide and 50 mg of polyvinylpyrrolidone K30 in 450 µl of ethylene glycol. The solution was stirred thoroughly until fully mixed. The ink was stored in the dark at 4 °C.

Preparation of the silver precursor

A silver precursor solution was prepared by dissolving 14.1 mg of silver nitrate and 13.4 mg of trisodium citrate in 1 ml of deionized water under vigorous stirring. Aqueous ammonia (25 wt%) was then added dropwise under continuous stirring until the solution became transparent, indicating complete complexation. After preparation, the solution was stored in a dark place.

2PP-based 3D printing of the OFG

Initially, a commercial optical fibre cleaver was used to produce a flat-end face on a multimode optical fibre. SZ2080 photoresist was applied onto the fibre-end face and cured by heating at 100 °C for 1 h on a hotplate. Using a custom-built femtosecond laser, two-photon polymerization 3D printing system, a rigid microclaw structure was fabricated at the fibre tip using 3D beam scanning. Following polymerization, the structure was immersed in ethanol for 1 h to remove residual, unpolymerized photoresist. The hydrogel precursor was subsequently applied to the claw structure, and a second 2PP step was performed for accurate spatial printing of the hydrogel component. The processed fibres, along with the photoresist and hydrogel materials, were then immersed in ethanol for 5 min to remove unpolymerized hydrogel material. Finally, the entire structure was placed in a prepared silver nitrate reduction solution and immersed for 5 min. Near-infrared laser light was introduced from one end of the optical fibre, transmitted through the fibre and irradiated the structure at the other end (Supplementary Video 2). This process induced a photochemical reduction reaction, depositing silver nanoparticles within the hydrogel material.

Cell culture

HeLa cells were obtained from Shanghai Priman Biotechnology and cultured in a humidified incubator at 37 °C and 5% CO_2. The cells were maintained in HeLa cell complete medium (CM-0101, Procell system). For single-cell manipulation experiments, the cells were detached using 0.25% Trypsin-EDTA (Gibco) at 37 °C for 30 s. The cell suspension was subsequently centrifuged at 150 × *g* for 5 min and resuspended in fresh medium to the desired density.

Characterization

SEM imaging was conducted using an EVO18 secondary electron system (ZEISS). Before imaging, the samples were critical-point dried and sputter-coated with an approximately 3–5 nm gold layer. Bright-field images were acquired using a Leica DMI 3000B inverted optical microscope. Energy-dispersive spectroscopy mapping was performed using cold-field emission SEM (Hitachi SU8220). Actuation dynamics were captured by a high-speed camera (Chronos 2.1-HD). The deformation of OFG was extracted from image sequences based on pixel coordinates and converted using the calibrated pixel-to-length ratio. Because pixel coordinates are discrete, the resulting deformation values are quantized, which can lead to repeated values and step-like changes in the source data.

Preparation of adhesive-modified samples

To capture the closed configuration of the OFG during sampling under SEM (Fig. 5i), we prepared samples with enhanced adhesion and allowed the OFG to sample them before dehydration. The sample was prepared as follows: carboxymethyl cellulose (50 mg), carrageenan (20 mg) and xanthan gum (80 mg) were weighed and mixed to homogeneity, followed by dropwise addition of glycerol (2,500 µl). Separately, calcium carbonate (3,000 mg) was ground in a mortar for 30 min to yield highly micronized particles, which were then incorporated into the mixture in three portions with thorough stirring after each addition. The final sample was obtained after sufficient homogenization.

Animal models and ethical approval

Freshly excised rabbit hepatobiliary tissues were obtained as by-products from commercially slaughtered New Zealand rabbits intended for food production, and live New Zealand rabbits were used for in vivo bile duct manipulation experiments. All procedures related to tissue procurement and all in vivo animal experimental protocols, including pain management, surgical procedures and humane euthanasia, were reviewed and approved by the Institutional Animal Care and Use Committee of the Shenzhen Advanced Medical Services (approval no. AASE2511013R).

Finite-element simulations

Multiphysics simulations were performed using finite-element analysis. The simulation model accounted for photothermal energy conversion, thermal conduction, hydrogel swelling–shrinkage and induced structural deformation. Additional simulation is provided in the Supplementary Information, Table 1, Section 3.

Data availability

Source data are provided with this paper. All other data that support the findings of this study are available from the corresponding authors upon reasonable request.

Acknowledgements We thank W. Xiong, C. Li, H. Hu, M. Zhang, Y. Zheng, X. Wu and Y. Yin for their assistance with material preparation and characterization. We acknowledge the Modern Experiment Technology Center of Anhui University and Experimental Center of Engineering and the Material Sciences at USTC for their support in sample fabrication and characterization. This work was partially carried out at the USTC Center for Micro and Nanoscale Research and Fabrication and Instruments Center for Physical Science, University of Science and Technology of China. The analysis work of this article was partially carried out at the Instrumental Analysis Center, Hefei University of Technology.

Author contributions D.P., Y.H. and D.W. conceived the project. D.P., D.W., K.L., C.X., L. Zhong, Z.W., S.Z., L.Y., J.N., C.Z., C.W. and Y.H. designed and carried out the experiments. D.P., D.W., S.J. and L. Zhong wrote the paper. C.W., J.L., B.Y., Y.H., Z.L., C.Z., Z.H., F.-W.S., J.C. and L. Zhang analysed the data. All authors participated in the discussion and contributed to the refining of the manuscript.

Funding This work was supported by the National Key Research and Development Program of China (nos. 2021YFF0502700 and 2024YFB4610700), the National Natural Science Foundation of China (nos. 62325507, 52375582, 62205236, 62461160305, 62275242, 62475066 and 62475252), the Suzhou Innovation Youth Leading Talent Project (ZXL2023158), the CAS Project for Young Scientists in Basic Research (no. YSBR-049), the Fundamental Research Funds for the Central Universities (WK2090050048 and WK2030000108), the Scientific Research Project of Anhui Provincial Department of Education (2025AHGXZK20171), and the Anhui Provincial Key Research and Development Program in Basic Field Projects (2023Z04020012).

Competing interests The authors declare no competing interests.

Additional information
Supplementary information The online version contains supplementary material available at https://doi.org/10.1038/s41586-026-10673-7.
Correspondence and requests for materials should be addressed to Chenchu Zhang, Chaowei Wang, Yanlei Hu or Dong Wu.
Peer review information *Nature* thanks Hao Zeng and the other, anonymous, reviewer(s) for their contribution to the peer review of this work. Peer reviewer reports are available.